ARTICLE

The AAV2.7m8 capsid packages a higher degree of heterogeneous vector genomes than AAV2

Mengtian Cui[1], Qin Su[1], Mitchell Yip[1], Jackson McGowan[1], Claudio Punzo[1,2], Guangping Gao[1,3]✉ and Phillip W. L. Tai[1,3]✉

Recombinant adeno-associated virus (rAAV) vectors are currently the only proven vehicles for treating ophthalmological diseases through gene therapy. A wide range of gene therapy programs that target ocular diseases are currently being pursued. Nearly 20 years of research have gone into enhancing the efficacy of targeting retinal tissues and improving transgene delivery to specific cell types. The engineered AAV capsid, AAV2.7m8 is currently among the best capsids for transducing the retina following intravitreal (IVT) injection. However, adverse effects, including intraocular inflammation, have been reported following retinal administration of AAV2.7m8 vectors in clinical trials. Furthermore, we have consistently observed that AAV2.7m8 exhibits low packaging titers irrespective of the vector construct design. In this report, we found that AAV2.7m8 packages vector genomes with a higher degree of heterogeneity than AAV2. We also found that genome-loaded AAV2.7m8 stimulated the infiltration of microglia in mouse retinas following IVT administration, while the response to genome-loaded AAV2 and empty AAV2.7m8 capsids produced much milder responses. This finding suggests that IVT administration of AAV2.7m8 vectors may stimulate retinal immune responses in part because of its penchant to package and deliver non-unit length genomes.

Gene Therapy; https://doi.org/10.1038/s41434-024-00477-7

INTRODUCTION

Adeno-associated viruses (AAVs) are small, single-stranded (ss) DNA viruses belonging to the *Parvoviridae* family. Recombinant (r) AAV vectors, which are removed of all viral genes are considered to be non-pathogenic. Moreover, compared to other viral vectors, rAAVs have low immunologic profiles [1]. These features have made rAAVs the most widely used vehicles in the gene therapy field, especially for treating ocular disease [2, 3]. rAAVs have demonstrated efficacy in clinical trials for inherited retinal dystrophies, including Leber's congenital amaurosis (LCA), choroideremia, and X-linked retinitis pigmentosa [4–6]. There is currently one FDA-approved gene therapy for LCA (Luxterna) [7, 8]. Despite the recent successes in the gene therapy field using rAAVs to target the liver, CNS, and striated muscle, some barriers still remain that hinder a wider application for eye gene therapy. Namely, rAAV administration via intraocular injection has been shown to trigger vasculitis or uveitis [9], limiting therapeutic efficacies for vectors and risking complications for patients [10]. Thus, a better understanding of rAAV-triggered immune responses is critical for improving safety and visual outcomes following retinal gene therapy.

Intravitreal (IVT) injections are among the most common ocular procedures used in the clinic and are routinely performed for anti-vascular endothelial growth factor (VEGF) therapies [1, 11–14]. However, IVT injections of rAAV have been reported to trigger inflammatory responses and can lead to the systemic biodistribution of vectors to lymph nodes [15]. This dissemination can, in turn, trigger neutralizing antibody responses towards the transgene. Moreover, there are several reports attributing immune responses to elements related to vector manufacturing, administration doses, certain vector capsids, and/or the promoters that control gene expression [15]. Other clinical factors, such as the patient's surgical history, age, pigmentation, an overactive immune system, human leukocyte antigen type, and the presence of neutralizing antibodies can also be drivers of gene therapy-related adverse effects [1, 16]. The current understanding in the ocular gene therapy field is that the AAV capsid is the most important factor in eliciting immune responses. For instance, cytokine factors increase in the mouse retina after IVT delivery of AAV5 and AAV8 capsids [9].

The most commonly used capsids for ocular gene therapy are AAV2, AAV2.7m8, and AAV8 [17]. AAV2.7m8 is an engineered capsid that carries an insertion of ten amino acids at each of the three-fold spikes of AAV2 [18] and was discovered by a "7-mer" library screen to identify capsids that can transduce mouse photoreceptor cells. It should be noted that the first three amino acids serve as a linker to permit the structural integrity of the 7-mer insert. The 7m8-defining residues (LALGETTRPA) are inserted at amino acid position 588 of the AAV2 VP1 capsid sequence, a location that is at the outermost protruding region on the capsid surface. The insertion also disrupts the basic arginine residues in hypervariable region VIII that are implicated in AAV2's binding to its primary receptor, heparan sulfate proteoglycan (HSPG) [19]. AAV2.7m8 also shows strong transduction of mouse inner ear tissues, implicating it as a promising vehicle for delivering therapeutic genes to prevent or reverse hereditary

[1]Horae Gene Therapy Center, UMass Chan Medical School, Worcester, MA, USA. [2]Department of Ophthalmology and Visual Sciences, UMass Chan Medical School, Worcester, MA, USA. [3]Department of Microbiology, UMass Chan Medical School, Worcester, MA, USA. ✉email: Guangping.Gao@umassmed.edu; Phillip.Tai2@umassmed.edu

Received: 4 April 2024 Revised: 3 August 2024 Accepted: 6 August 2024
Published online: 12 August 2024

hearing loss [20]. Although the 7m8 modification on AAV2 shows significant improvement in retinal transduction, we have found that the capsid inherently produces lower titers compared to other serotypes, which is consistent with the literature [21].

Importantly, delivery of AAV2.7m8 into non-human primates (NHPs) has been shown to trigger adverse effects. Severe chronic inflammation was observed following subretinal injection of AAV2.7m8 at a dose of 1E + 12 vg/eye. Similarly, intravitreal (IVT) injection of AAV2.7m8 at high doses (1E + 12 vg/eye) resulted in retinal infiltrates, with no choroidal observed inflammation [22]. AAV7m8 was also reported to lead to retina and RPE toxicity after subretinal injections in mouse models [9]. Critically, there have been a handful of reports showing AAV2.7m8-related clinical adverse effects or even vision loss after treatments. For example, a clinical trial for wet age-related macular degeneration (AMD) (NCT04418427), which used the AAV2.7m8 capsid to deliver an anti-VEGF transgene, described the occurrence of ocular vasculitis with an associated decrease in vision [23–25]. These findings suggest that the administration of rAAV2.7m8-based gene therapy may carry severe adverse inflammatory events in patients. Consequently, anti-inflammatory interventions are needed to mitigate or eliminate inflammatory responses following administration [26–28].

To better understand the poor production of AAV2.7m8-based vectors and their consequences for stimulating inflammation during retinal transduction, we performed head-to-head comparisons between AAV2 and AAV2.7m8 vectors. We found clear differences in purified vectors, where AAV2.7m8, irrespective of the vector genome design, showed poorly defined bands during the CsCl ultracentrifugation steps, suggesting at the presence of heterogenous vector populations. Using AAV Genome Population sequencing (AAV-GPseq) [29], we found that AAV2.7m8 packaged a higher degree of non-unit length genomes than AAV2. To determine whether vector genome heterogeneity is the driving factor in triggering retinal immune responses, AAV2 and AAV2.7m8 vectors produced with an enhanced green fluorescent protein (*Egfp*) expression cassette (full capsids), or without vector genomes (empty capsids) were IVT injected into mouse eyes. We observed that AAV2.7m8 stimulated the infiltration of microglia in mouse retinas following delivery, while the response to AAV2 was much milder. Notably, administration of empty AAV2 and AAV2.7m8 particles resulted in even milder responses compared to genome-loaded vectors. These findings suggest that AAV2.7m8 tends to package truncated genomes and suggest that these species are a causative factor in AAV2.7m8's penchant to stimulate immune responses in treated eyes.

MATERIALS AND METHODS

Plasmid and vector production

The AAV2.7m8 *trans* plasmid construct, previously described by others [18], was obtained from Addgene (plasmid #64839). All *cis*-plasmid constructs described in this manuscript were obtained from stocks provided by the UMass Chan Viral Vector Core and were quality checked by Nanodrop and standard restriction digest with *Sma*I and gel electrophoresis. Large-scale production of the helper plasmid (pAdDeltaF6) and AAV2 *trans* plasmids were ordered from Aldevron. The *trans* and *cis* plasmids described in this study were sourced from either in-house CsCl production or commercially ordered (Table S1). Vectors were produced using the triple-plasmid transfection method in HEK293 cells and purified by CsCl gradient ultracentrifugation as described previously [30]. Vectors were aliquoted into 200 µl stocks and stored at −80 °C immediately after production. Thawed aliquots were kept at 4 °C before use and warmed to room temperature before injection. All AAV2 or AAV2.7m8 vectors described were packaged with a self-complementary vector ubiquitously expressing EGFP (scAAV-*CB6-Egfp*), a single-stranded vector expressing firefly luciferase (ssAAV-*CB6-FLuc*), or an ssAAV vector expressing EGFP (ssAAV-*CB6-Egfp*). Crude lysates were obtained from small-scale production in HEK293 cells by triple-plasmid transfection [31]. After three days of culturing, cell lysates were subjected to three freeze-thaw cycles. Cell debris was removed by centrifugation and the supernatants were used for the titration of vectors. The titrations reported in this study were performed by ddPCR [32] using probes against *Egfp* (Thermo Fisher Scientific, Mr04329676_mr) or *nRGB* (Fwd: GCCAAA AATTATGGGGACAT, Rev: ATTCCAACACACTATTGCAATG, and TaqMan probe: 6FAM-ATGAAGCCCCTT GAGCATCTGACTTCT-TAMRA). Probes and primers were synthesized by Integrated DNA Technologies. Empty capsids were titrated by semi-quantitative analyses of VP1/2/3 protein abundances with SDS-PAGE and silver staining as described below.

Silver staining

AAV particles were loaded onto 4–12% Bis-Tris protein gels (NuPAGE, Invitrogen) for electrophoretic separation and stained using the SilverXpress™ kit (Thermo Fisher Scientific) as described previously [33]. Protein bands were visualized and quantified by comparing to a VP1/2/3 capsid standard on a ChemiDoc MP Imaging system (BioRad).

Vector DNA extraction and agarose gel electrophoresis

AAV vector genomes were extracted for preparations using phenol:chloroform:isoamyl alcohol (25:24:1) and ethanol precipitation as described previously [29]. Briefly, samples underwent heating and strand annealing in annealing buffer (25 mM NaCl, 10 mM Tris-HCL [pH 8.5], 0.5 mM EDTA [pH 8.0]) at 95 °C for 5 min and cooled to 25 °C (1 min for every −1 °C) on a thermocycler (Eppendorf Mastercycler). Purified vector DNAs were then subjected to denaturing alkaline gel electrophoresis. Gels were stained with ethidium bromide to visualize.

SMRT sequencing and AAV-GPseq

Purified vector DNAs were processed for single molecule, real-time (SMRT) sequencing by the UMass Chan Medical School Deep Sequencing Core. Libraries for vector DNAs were constructed using the Express Template Prep Kit 2.0 (End Repair/A-tailing) (PN 100-938-900) and ligated to indexed SMRT bell adapters with the Barcoded Overhang Adapter Kit (PN 101-628-400/500). Libraries were pooled and purified using 1.8× AMPure beads. Sequencing was performed on a Sequel II instrument. Subreads from each library underwent preprocessing steps prior to analysis as described previously [34]. Briefly, subreads were first processed through recalladapters 9.0.0 with the following parameters: --minSnr = 2.0 and --disableAdapterCorrection. This step recovered long palindromic sequences that were artificially cleaved from subreads generated by SMRT Link (v12). Subsequent subreads were then processed using the circular consensus sequencing (CCS) tool in SMRT Link version 12.0.0 with the following parameters: --minSnr = 3.75, --min = passes = 2.0, and --by strand. The following bioinformatic workflows were conducted using the Galaxy platform [35, 36]. Resulting consensus fastq files were mapped to the references as reported in the study using the Burrows–Wheeler aligner-maximal exact match (BWA-MEM) [37, 38] in PacBio mode (-x pacbio). Aligned reads were visualized with the Integrated Genomics Viewer (IGV) tool version 2.14.0 [39] with soft clipping on.

Animals

Four- to five-week-old female C57BL/6 J mice (The Jackson Laboratory) were injected by IVT administration. Mice were kept on a 12 h light/12 h darkness light cycle, at 70–74 °F with 35–46% humidity. Mice were fed normal chow (ISO-pro 300 Irradiated Diets (#5P76)). All animal procedures described in this study were approved by the UMass Chan Medical School Animal Care and Use Committee.

IVT injections

IVT injections were performed with glass needles (Clunbury Scientific LLC; Cat no. B100-58-50) to deliver ~1 µL of fluid into the vitreous using the FemtoJet from Eppendorf with a constant pressure and injection time of 300 psi and 1.5 s, respectively. Mice were administered with vectors packaged with scAAV2-*CB6-PI-Egfp* or scAAV2.7m8-*CB6-PI-Egfp* transgenes (1.0E9 vg per mouse), and mice were sacrificed six weeks post-injection. Animals were not randomized and not blinded in the study and were injected according to cage group.

Immunohistochemistry

Treated retinas were cryosectioned as previously described [13]. In brief, eye cups were dissected in cold 1× phosphate-buffered saline (PBS) and fixed in 4% paraformaldehyde overnight at 4 °C. Cryosections were cut at a

thickness of 12 µm. The following primary antibodies and dilutions were used: chicken anti-EGFP antibody (1:1000; Abcam; Cat no. ab13970), and rabbit anti-IBA1 (1:300; Wako; Cat no. 019-19741). The chromophore conjugate, fluorescein peanut agglutinin lectin (PNA) (1:1,000; Vector Laboratories; Cat no. FL1071) was used to stain cone photoreceptors. All antibodies were diluted in PBS with 0.3% Triton X-100 and 5% bovine serum albumin (CST). Nuclei were counterstained with 4′,6-diamidino-2-phenylindole (1:2000, Sigma–Aldrich; Cat no. 9542). All secondary antibodies (1:1000, donkey) were purchased from Thermo Fisher Scientific. All images were visualized with a Leica DM6 Thunder microscope with a 16-bit monochrome camera. Images were processed by LAS X Life Science Microscope Software.

Statistical analyses

One-way or two-way ANOVA with Tukey's method for multiple comparisons given equal variance was used as indicated. A p-value of <0.05 was considered statistically significant and plotted accordingly. Sample sizes of relevant data reported in this study provide adequate power but were not pre-specified.

RESULTS

AAV2.7m8 preparations consistently yield undefined bands and fewer full-length genomes

Motivated by evidence that AAV2.7m8-based vectors yield lower titers when produced by standard triple-plasmid transfections, we packaged the *Egfp* transgene cassette driven by the ubiquitous CMV-enhancer/chicken-actin hybrid promoter (*CB6*) and bovine growth hormone polyadenylation (*BGH*-polyA) into AAV2 and AAV2.7m8 capsids. In addition, both scAAV and ssAAV forms (2.1 kb and 2.3 kb, respectively) were produced (Fig. 1a). We also packaged an ssAAV vector containing a firefly luciferase (*FLuc*) transgene cassette driven by the same promoter (Fig. 1a). As part of the production workflow, vectors were subjected to CsCl density gradient ultracentrifugation to isolate full capsids from empty capsids (Fig. 1b). During this step, we observed that each of the preparations exhibited a visible and defined low molecular weight band, representing empty capsids. The high molecular weight band, representing full capsids, was well-defined for ssAAV2-*Egfp* and ssAAV2-*FLuc* vectors but was ill-defined for scAAV2-*Egfp* and all AAV2.7m8 capsid-related preparations. Notably, the scAAV2.7m8-*Egfp* and ssAAV2.7m8-*Egfp* vectors lacked any distinguishable full capsid bands. These vectors instead displayed smears (Fig. 1b), which typically indicates a high degree of heterogeneous "intermediate" species [29].

After purification, we found that there were no major differences in the titers obtained by ddPCR quantification (Table S1). In fact, the AAV2.7m8 vectors tended to have higher titers than those of the AAV2 vectors. Silver-stained gels of the scAAV2-*Egfp* and scAAV2.7m8-*Egfp* did not reveal any major capsid-related differences, aside from the anticipated higher molecular weight shift in the AAV2.7m8 capsid caused by the 10-amino acid insertion (LALGETTRPA, 1.03 kDa) (Fig. S1). The expected distribution of the capsid proteins (i.e., the approximate 1:1:10 ratio of VP1, VP2, and VP3) was similar between AAV2 and AAV2.7m8.

We predicted that the vector smears observed among the AAV2.7m8 vectors in the CsCl gradients were attributed to non-unit length and/or truncated genomes. To determine whether vectors produced with AAV2.7m8 packaged a higher degree of heterogeneous genomes, we directly examined DNase-resistant genomes from crude lysates obtained from small-scale packaged vectors by multiplex Droplet Digital PCR (ddPCR) (Fig .1c). Using ddPCR probes targeting the *CB6* promoter and the *Egfp* transgene, we found that vectors packaged with AAV2.7m8 showed an overall lower percentage of double-positive droplet reads (i.e., positive *CB6* and *Egfp* probe signals), than those packaged with AAV2 (Fig. 1c). The scAAV2 vector showed 73.1% double-positive droplets, while scAAV2.7m8 showed 46.4% double-positive droplets. Similarly, the ssAAV2 vector showed higher double-positive droplets than observed for the ssAAV2.7m8 vector (48.4% versus 26.0%) (Fig. 1c).

To validate that the AAV2.7m8 capsid packages a higher degree of truncated genomes, we isolated vector DNA from CsCl density gradient ultracentrifugation-purified vectors and subjected them to alkaline (denaturing) gel electrophoresis analyses (Fig. 1d). All of the preparations had predominant bands attributed to the full-length vector genome. It should be noted that since sc genomes package both plus and minus stranded genomes as an unresolved dimer, full-length sc genomes are expected to migrate at approximately double the size of the design in alkaline gels. Therefore, the 2.1-kb scAAV-*CB6-Egfp* design should migrate at approximately 4.2 kb. Interestingly, the scAAV2-*Egfp* and scAAV2.7m8-*Egfp* vectors displayed multiple minor bands at ~5.0 kb, ~3.0 kb, and ~2 kb (Fig. 1d). The scAAV2.7m8-*Egfp* vector showed additional bands at ~1.0 kb and a very faint band at ~0.5 kb. The ssAAV2-*Egfp* and ssAAV2.7m8-*Egfp* showed prominent bands at just under 5 kb in size. We predicted that this band represents unresolved sc forms. We have noted that ssAAV vectors can package scAAV forms [29], especially if the size of the unresolved dimer is less than 4.7 kb. We also noticed several additional smeary bands residing between 1 and 2 kb in size (Fig. 1d). Finally, the ssAAV2-*FLuc* vector displayed a high degree of homogeneity. In contrast, the ssAAV2.7m8-*FLuc* vector exhibited six distinct minor bands (Fig. 1d). These results demonstrate that vectors packaged with the AAV2.7m8 capsid tended to package a higher degree of non-unit length forms.

We also asked whether other 7-mer inserts could result in the packaging of non-unit length genomes. In the report first describing AAV2.7m8, three additional retinotropic 7-mer peptide inserts (LAKDPKTTN, LAKAGQANN, and LANETITRP), were also examined [18]. We, therefore, synthesized these and renamed them AAV2.7 mA, AAV2.7mB, and AAV2.7mC, respectively. To examine their capacity to impact the packaging of non-unit length/truncated genomes, we produced vectors with scAAV-*CB6-Egfp* transgene cassettes, isolated DNase-resistant vector genomes, and ran them on alkaline gels (Fig. 2a). We also observed that the genomes of all three vectors exhibited non-unit length species similar to those observed with AAV2.7m8. This data suggested that other 7-mer inserts with the AAV2 capsid might also compromise vector genome integrity. Recent studies have also used AAV9 as the bases for 7-mer peptide screens [40, 41]. To probe whether 7-mer insertions affect AAV9 in the same manner, we obtained MyoAAV-*CB6-mCherry* and AAV9.PHP.eB-*CB6-Egfp* vectors, both have 7-mer peptides inserted within hypervariable region VIII between residues 588 and 589 [41, 42], the same locale as the 7m8 insertion within AAV2 [18]. We isolated their vector genomes and subjected them to alkaline gel analyses. Compared to its AAV9 counterpart, we observed very little difference in the abundance of non-unit length genomes for MyoAAV (Fig. 2b). When AAV9 is packaged with the ss*CB6-Egfp* transgene cassette, two prominent bands are observed, one at ~2.3 kb (the expected full-length monomer size) and one at ~4.2 kb (the approximate size of an unresolved dimer). Two additional fainter bands were also observed, one at ~3 kb and one at 5 kb. The 3-kb band is attributed to snap-back genomes centered on the *CB6* promoter, as reported previously [29, 43]. The 5-kb band represents oversized species of unresolved genomes that have reached the packaging limit. Importantly, the AAV9.PHP.eB-packaged vector seemed to have a visible band at ~1.6 kb, which was not prominently found for the AAV9-packaged vector (Fig. 2c). These data suggest that 7-mer insertions may only substantially affect vector genome integrity for AAV2.

AAV-GPseq reveals that AAV2.7m8-packaged vector genomes have a higher degree of truncated genomes than AAV2-packaged vectors

We next aimed to profile the non-unit length genomes revealed among AAV2.7m8-packaged vectors (Fig. 1d). We previously

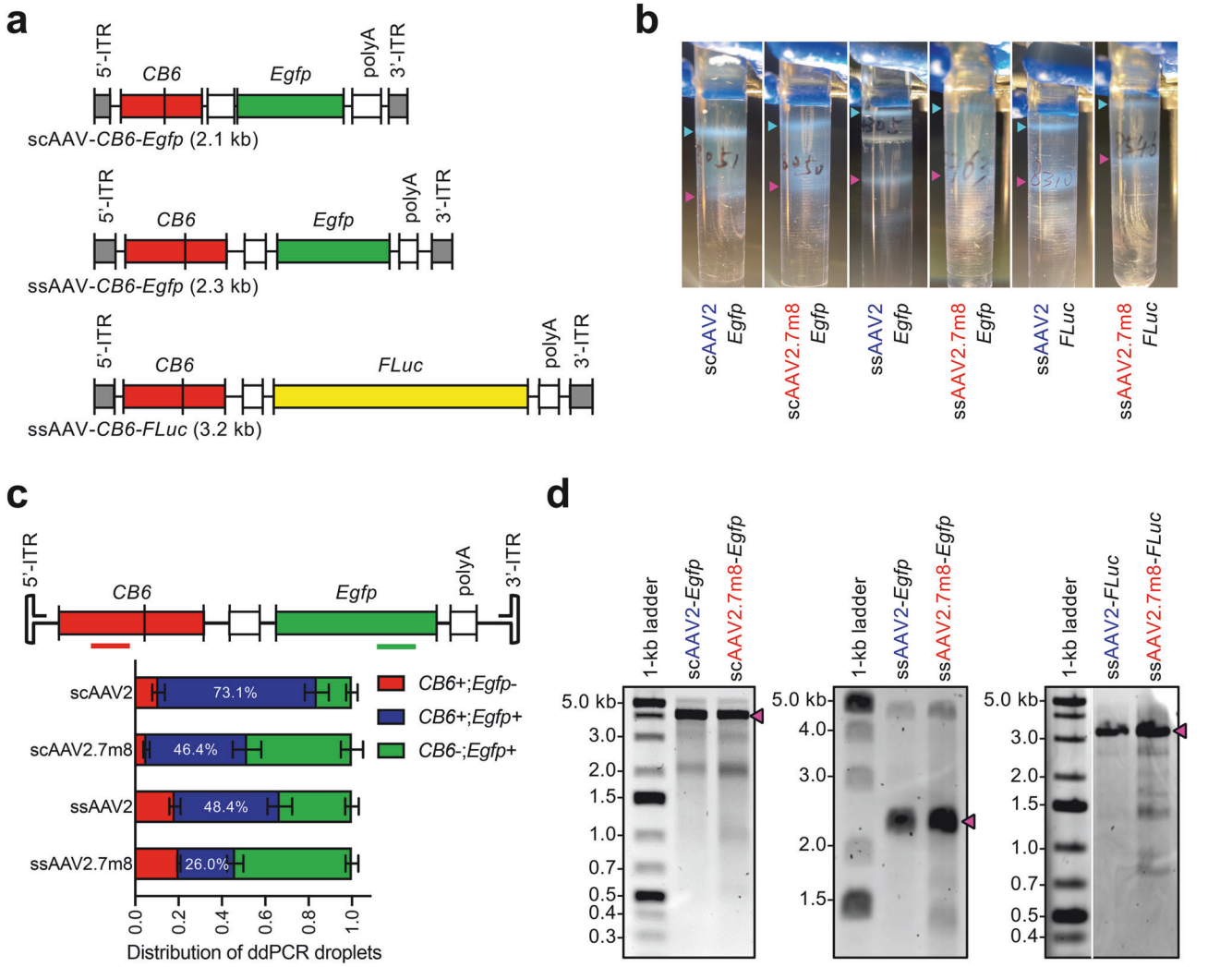

Fig. 1 Production and analyses of AAV2 and AAV2.7m8 test vectors. a Diagrams of self-complementary (sc)AAV-*CB6-Egfp*, single-strand (ss) AAV-*CB6-Egfp*, and ssAAV-*CB6-FLuc* vectors. **b** Photographs of the three vectors subjected to CsCl density gradient ultracentrifugation. Bands representing empty capsids (light-blue arrowheads) and full capsids (purple arrowheads) are indicated. **c** ddPCR quantification of scAAV-Egfp and ssAAV-Egfp vectors using probe sets against the *CB6* promoter and the *Egfp* transgene displayed as a stacked histogram. Detection of *CB6*-only (red) or *Egfp*-only (green) droplets indicate partial genomes, while detection of both CB6 and *Egfp* (blue) species suggests the presence of full-length genomes. Values represent mean frequencies ± SD, ($n = 3$). The mean percentages of droplets double positive for *CB6* and *Egfp* probe signals are shown. Diagram of the vector genome target with the approximate position of the probes is shown above. **d** Alkaline gels for AAV2 and AAV2.7m8 vectors packaged with scAAV-*CB6-Egfp* (left), ssAAV-*CB6-Egfp* (center), and ssAAV-*CB6-FLuc* (right). Bands predicted to contain unit length genomes are marked with purple arrowheads.

developed a long-read sequencing method, based on Pacific Biosciences' single-molecule real-time (SMRT) sequencing approach, called AAV-GPseq to specifically profile truncated genomes in AAV vector preparations [29]. Therefore, DNase-resistant genomes were subjected to this analysis to characterize the composition of scAAV-*CB6-Egfp*, ssAAV-*CB6-Egfp*, and ssAAV-*CB6-FLuc* genomes when packaged by AAV2 or AAV2.7m8 (Fig. 3).

Alignment of sequencing reads obtained from the sc*CB6-Egfp* cassette packaged with AAV2 to the *cis*-plasmid reference revealed that the dominant species were full-length sc vector genomes (~4.2 kb), as expected (Fig. 3a). A smaller portion of truncated species, as well as ss forms, were also present. Importantly, reads from the same cassette packaged by AAV2.7m8 also showed predominantly sc vectors, but a higher abundance of truncated genomes was revealed. These differences were also revealed when plotting the read counts as a function of their lengths (Fig. 3b). Vector genomes packaged by AAV2.7m8 showed a higher proportion of reads under 1.5 kb in length. This finding coincides with the presence of <1.5 kb bands revealed by alkaline gels (Fig. 1d).

When reads from the ss*CB6-Egfp* vector packaged with AAV2 were mapped to the *cis*-plasmid, the alignments showed that they predominantly spanned from ITR-to-ITR (Fig. 3c). However, we observed two populations, one at the expected length of 2.3 kb, and a second with lengths that were double the size (~4.6 kb) (Fig. 3d). These longer reads represent unresolved sc forms, which coincide with the high molecular weight band observed in the alkaline gel for this vector preparation (Fig. 1d). Interestingly, reads from the vector packaged with AAV2.7m8 exhibited a high abundance of short <2 kb reads (Fig. 3d). These reads also coincided well with alkaline gels of the ss*CB6-Egfp* vector packaged with AAV2.7m8 (Fig. 1d). Furthermore, the expected 2.3-kb length reads were in the minority (Fig. 3d).

We also observed similar trends with reads representing the ss*CB6-FLuc* vector construct packaged into AAV2 and AAV2.7m8 (Fig. 3e, f). The predominant read species from the

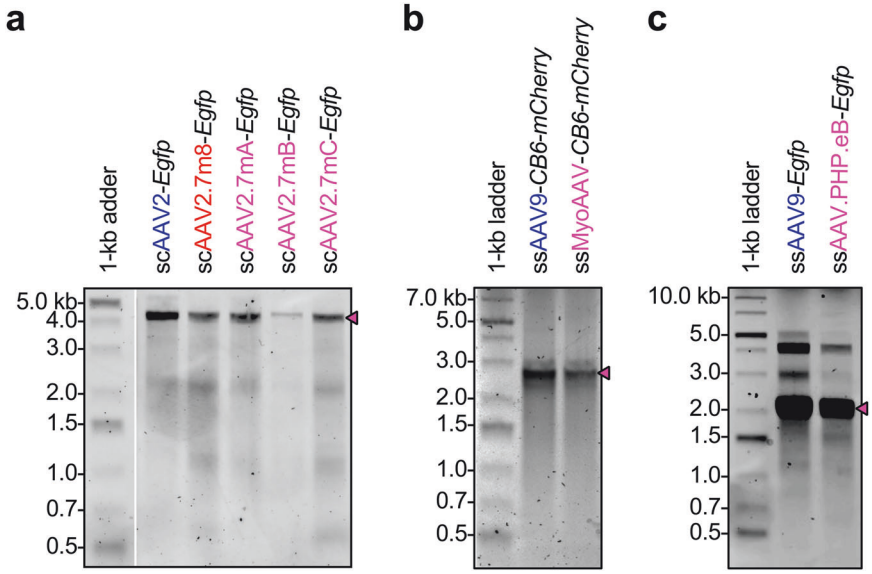

Fig. 2 7-mer inserts with AAV2 drive the packaging of non-unit length vector genomes, but not with AAV9. DNase-resistant genomes were isolated from vectors and ran on alkaline gels. Gels for sc*CB6-Egfp* vectors packaged with AAV2 and three additional retinotropic 7-mer peptide insert capsids (**a**), for ss*CB6-mCherry* vectors packaged with AAV9 or MyoAAV capsids (**b**), and for ss*Egfp* vectors packaged with AAV9 or AAV9.PHP.eB capsids (**c**) are displayed. Each gel was accompanied by a 1-kb DNA ladder. The expected full-length genome bands are marked with magenta arrowheads.

AAV2-packaged vectors was associated with the full-length 3.2-kb genome; while short, <2-kb reads were the dominant species for the AAV2.7m8-packaged vectors. We found that the short reads associated with truncated/snap-back genomes found with the ss*CB6-FLuc* vector were similar between AAV2- and AAV2.7m8 vectors. This observation suggests that the 7m8 modification itself does not cause the formation of truncation events; rather, truncation events for AAV2.7m8-packaged vectors were more prominent than with the AAV2-packaged vectors. Curiously, we detected a high abundance of reads representing oversized genomes (~6.4 kb) (Fig. 3f), especially for the AAV2 vector. Genomes greater than 5 kb were not observed in our alkaline gels (Fig. 1d), suggesting that the detection of these oversized genomes may be a result of library preparation bias and an artifact of the read length normalization process (see Materials and Methods). These species likely represent unresolved self-complementary genomes that may have survived the Benzonase endonuclease and DNase treatment steps [44]. Nevertheless, we found by AAV-GPseq that vectors packaged with AAV2.7m8 tended to yield a higher degree of truncated/snap-back genomes than those produced with AAV2.

Vector genome-loaded AAV2.7m8 stimulates infiltration of microglia in vector-treated mouse retinas

To understand the impact of delivering vectors that package truncated genomes, we administered scAAV2-*Egfp* or scAAV2.7m8-*Egfp* vectors into mouse eyes by IVT injection at 1E9 vg/eye. It should be noted that EGFP protein on its own is not known to stimulate strong immune responses in mouse eyes following IVT injection [9]. We also injected mice with empty AAV2 and AAV2.7m8 capsids (1E9 vp/eye) to determine whether the capsids alone can stimulate immune responses. After six weeks post-injection, treated mice were sacrificed, and their retinas were harvested. To evaluate immune responses toward vector treatment, we stained-cryosectioned retinas with anti-IBA1 (Fig. 4), which stains microglia, the resident immune cells of the retina that is used as a marker for immune responses in AAV-treated eyes [9, 13, 45]. Qualitative comparisons between retinas treated with empty AAV2 or AAV2.7m8 capsids revealed lower IBA1 staining than in retinas treated with capsids packaged with scCB6-*Egfp* cassette (Fig. 4a, b). Furthermore, we found that there was a higher abundance of IBA1+ cells at the ganglion cell layer (GCL) of eyes treated with capsids loaded with vector genomes. Notably, the GCL exhibits the strongest transduction by either AAV2 or AAV2.7m8 (Fig. 4b). Tabulation of IBA-stained cells in retinal cross-sections showed that eyes treated with empty capsids did not demonstrate a significant difference in microglia than retinas from eyes injected with saline solution (Fig. 4c). In contrast, retinas treated with scAAV2.7m8-*Egfp* showed ~47% more microglia than in retinas treated with scAAV2-*Egfp*.

The AAV2.7m8 capsid was originally identified for its ability to transduce mouse photoreceptor cells following IVT delivery through the penetration of the outer retinal cell layers. We surmised that AAV-triggered inflammation should result in microglia migrating and proliferating into the outer layers, beyond the outer plexiform layer (OPL). In the normal eye, microglia are radially distributed from the GCL interface and are mainly colonized at the inner plexiform layer (IPL) and OPL [46]. To determine whether microglia stimulation brought on by treatment with scAAV2.7m8-*Egfp* also increased migration/proliferation of microglia, we counted IBA1+ cells in treated retinas at each of the established retinal layers: GCL, IPL, inner nuclear layer (INL), OPL, outer nuclear layer (ONL), and the photoreceptor segment (PS) layer (Fig. 4d). We noted that vector genome-loaded vectors showed more microglia within the OPL, ONL, and PS layers. To assess the migration and localization of microglia across all of the retinal layers, we calculated the percentage of IBA1+ cells at each layer among all IBA1+ cells of the entire cross-section and compared them across treatment groups (Figs. 4d and S2). We found that the percentage of microglia at the GCL was slightly lower in the empty AAV2.7m8 capsid-treated retinas than observed with empty AAV2 capsids-treated retinas ($p < 0.05$) (Fig. S2). A similar trend was found in retinas treated with AAV2-*Egfp* versus scAAV2.7m8-*Egfp* ($p < 0.01$). When comparing retinas treated with empty AAV2.7m8 capsids and scAAV2.7m8-*Egfp* vectors, we found a lower percentage of IPL-localized microglia in eyes treated with empty particles than those packaged with genomes ($p < 0.01$). Furthermore, we observed losses in the percentage of INL-localized microglia in all AAV-treated retinas. Although we observed clear increases in

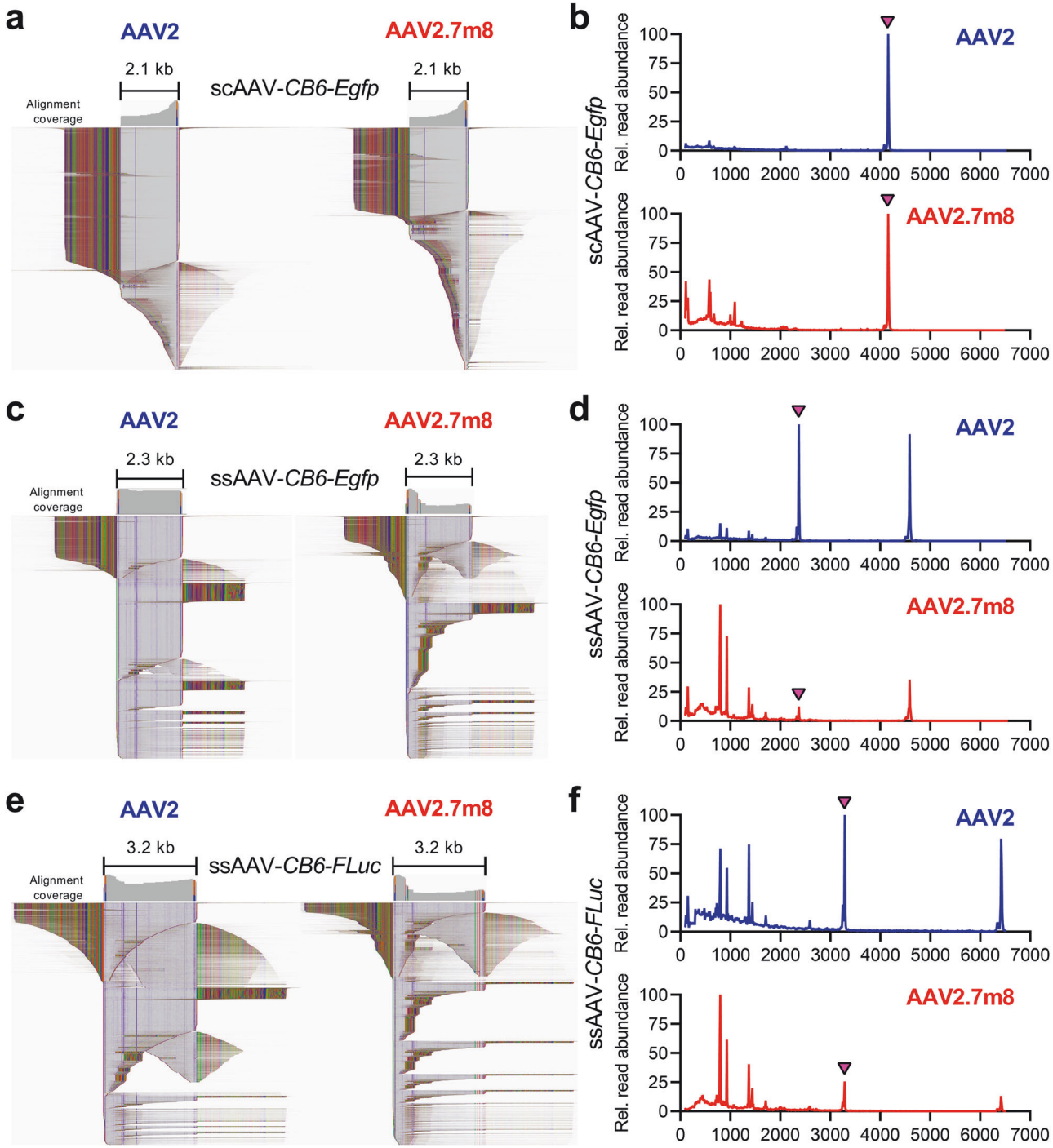

Fig. 3 AAV-GPseq analyses of vector genomes packaged with AAV2 and AAV2.7m8 capsids. a, **c**, **e** IGV displays of SMRT sequencing reads representing scAAV-*CB6-Egfp* (**a**), ssAAV-*CB6-Egfp* (**c**), *and* ssAAV-*CB6-FLuc* (**e**) vector genomes packaged into AAV2 (left) or AAV2.7m8 (right) aligned to their respective *cis*-plasmid references. Alignments are shown in squished displays with soft-clipped bases shown. Regions of read matches (gray), mismatches (colored), and insertions/deletions (speckles) are shown. Alignment coverages are shown above each display. **b**, **d**, **f** Traces of relative read abundances as a function of read length for scAAV-*CB6-Egfp* (**b**), ssAAV-*CB6-Egfp* (**d**), *and* ssAAV-*CB6-FLuc* (**f**) vector genomes packaged with AAV2 (blue traces) or AAV2.7m8 (red traces). The read lengths are normalized and scaled to the highest peak set to 100. Counts are binned into 10-nt distributions. Peaks representing the expected full-length genomes are marked with a purple arrowhead.

microglia in the ONL and PS among scAAV2-*Egfp*- and scAAV2.7m8-*Egfp*-treated retinas, we did not find significant changes when compared to saline and empty capsid groups (Fig. S2). This lack of support was mainly due to the relatively small number of IBA+ cells found in these layers, which did not permit statistical analyses. Nonetheless, the increased number of IBA1+ cells found in these outer layers (Fig. 4b, d) suggests that AAV2.7m8 vectors induced a higher level of inflammation compared to AAV2 vectors. Furthermore, we demonstrated that transgene-related inflammation in deep retinal layers is dependent on the presence of the transgene and not solely due to a capsid-related immune response.

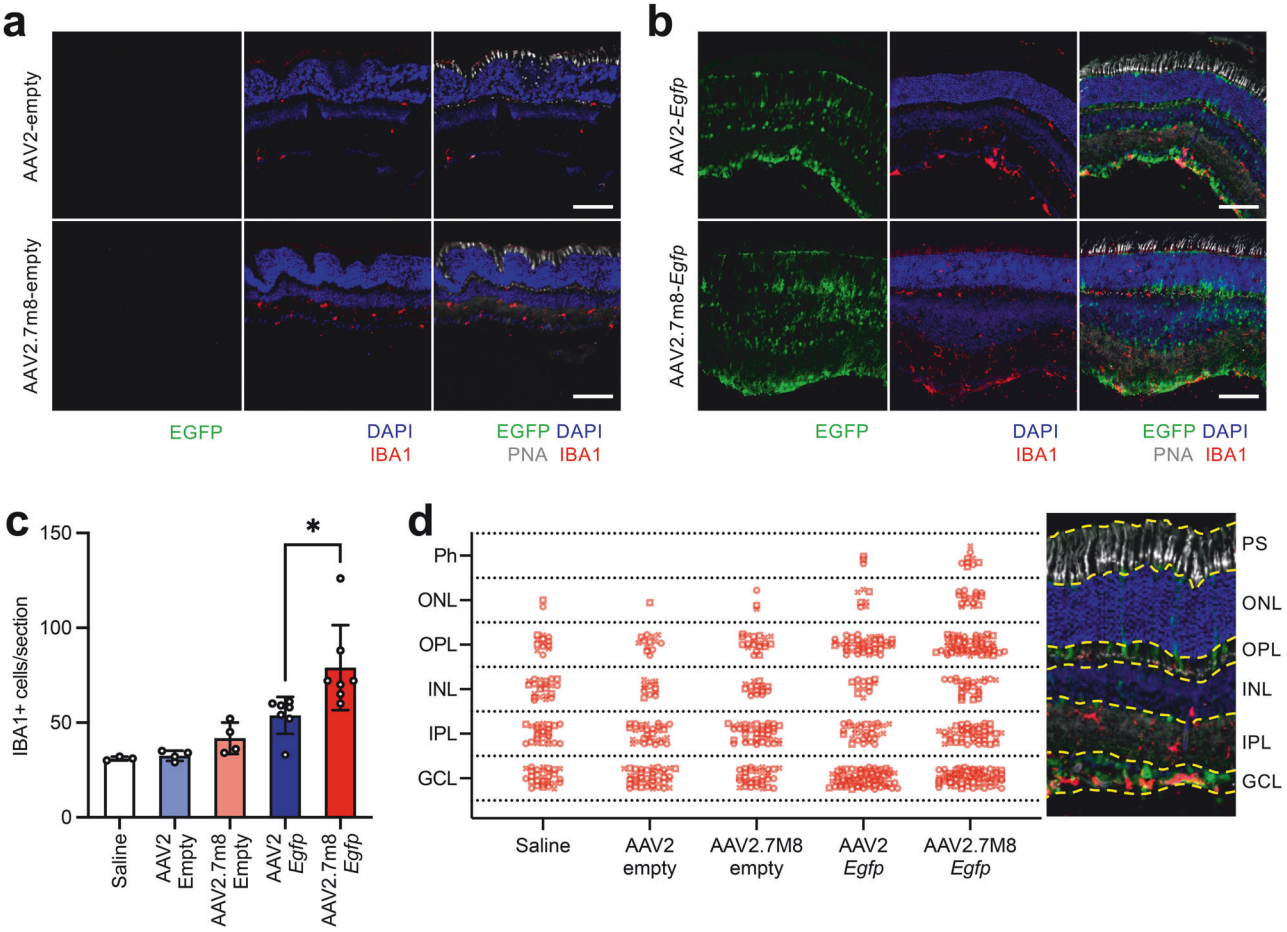

Fig. 4 Quantification of microglia in capsid/vector-treated retinas. a, **b** Immunofluorescence imaging of representative retinal cross-sections from mouse eyes IVT injected with empty AAV2 or AAV2.7m8 capsids (**a**), and eyes injected with scAAV2-*Egfp* or scAAV2.7m8-*Egfp* vectors (**b**). Sections were stained to visualize EGFP (anti-EGFP, green), DNA (DAPI, blue), cone photoreceptors (PNA, white), and microglia (IBA1, red). Scale bar = 100 μM. **c** Quantification of IBA+ cells in capsid/vector-treated retinas. Saline group, $n = 3$; empty capsid groups, $n = 5$; *Egfp* vector groups, $n = 7$. *$p < 0.05$, one-way ANOVA with Tukey's method for multiple comparisons. **d** Counts of microglia (IBA1+) in each retinal layer were tabulated for three cross-sections from different eyes of each treatment group. Photoreceptor segment layer (PS); outer nuclear layer (ONL); outer plexiform layer (OPL); inner nuclear layer (INL); inner plexiform layer (IPL); ganglion cell layer (GCL); shapes (circles, squares, and Xs) represent counts from each cross-section. The plot is accompanied by an example cross-section of a vector-treated retina (scAAV2-*Egfp*) to indicate layers of the retina.

DISCUSSION

Factors that contribute to vector heterogeneity are critically important to define. In our investigation, we addressed whether AAV2.7m8 has inherent production issues as observed in our own work and by others [21]. Although we did not find major differences between AAV2 and AAV2.7m8 in terms of titers for the vector constructs used in our examination (Table S1), our results showed that vector genomes packaged by AAV2.7m8 had a higher degree of truncated genomes (Fig. 3). These findings are significant since vectors that contain a high percentage of truncated genomes will deliver fewer functional transgenes than a vector that is packaged with a higher proportion of full-length genomes at equal vector genome doses. In other words, vectors with truncated genomes may not produce accurate functional titers. Although our conclusions were based on only three vector designs, the direct comparisons using the same vector construct packaged into either AAV2 or AAV2.7m8, highlight a new fundamental concept in AAV vectorology: that vector integrity can be impacted by the capsid. This in turn has direct implications towards the potency, efficacy, and safety of a gene therapy platform. Importantly, our study demonstrates the need to evaluate engineered AAV capsids for their ability to retain packaging integrity.

Another consideration for the data presented here is that the vectors were prepared by CsCl density gradient ultracentrifugation. We note that this method for purification is rarely used for clinical vectors, despite it being a superior approach for removing empty and intermediate capsids. Immuno-affinity column purification methods are currently the standard for clinical vectors, in part because CsCl density gradient ultracentrifugation purification cannot be scaled. It is important to note that vector genome heterogeneity is still present in column-purified vector preparations. In fact, we have found that the degree of genome heterogeneity is indiscriminately higher in affinity column-purified preparations [34] because discrete full capsid bands are not specifically identified and isolated during the purification process. Thus, we suspect that the observations made for AAV2.7m8's penchant to package higher degrees of truncated genomes compared to AAV2 would occur irrespective of purification methods.

As the most commonly used vectors for retinal gene therapy, AAV vectors have been widely reported for causing immunogenicity and inflammation in animals and humans through subretinal injection. Multiple variables can contribute to retinal toxicity following gene therapy: the presence of endotoxin in vector stocks, high empty/full of capsids, the promoter that is used to

drive transgene expression, the route of administration, and the vector dose [9, 15, 47]. In light of the adverse effects reported in clinical trials that have employed AAV2.7m8 capsids [24, 25, 48], our results indicate that immune responses towards AAV vectors may in part be due to heterogeneity in the vector genomes, rather than the capsid protein or the expected transgene product. Several reports have shown immune responses and/or toxicities from genomic contaminants that may result in the expression of unintended epitopes [49–51]. It remains unknown whether truncated genomes can stimulate innate immune responses, such as TLR9 activation through the detection of unmethylated CpG dinucleotides [52, 53], unfolded protein responses [54], or DNA/RNA sensing mechanisms [55]. Certainly, truncations in vectors can inadvertently increase CpG content in packaged vectors [34]. A study in NHPs has shown that AAV2.7m8 can cause higher cytokine responses than with other serotypes [22]. These outcomes have called into question the safety and efficacy of AAV2.7m8 [22].

Whether these immune responses can be a result of vector genome heterogeneity has been largely unexplored. In this study, we compared the inflammatory responses in retinas treated with empty AAV.7m8 capsids versus AAV.7m8-CB6-*Egfp* by IVT delivery. We showed that when AAV2.7m8 is packaged with the *CB6-Egfp* transgene cassette, it activated a higher number of microglia in transduced retinas than by empty AAV2.7m8 capsids (Fig. 4). Moreover, more microglia migrated into the outer retinal layers of eyes treated with the AAV2.7m8-*Egfp* vector than in eyes treated with empty AAV2.7m8 capsids or with AAV2-*CB6-Egfp*. These data collectively suggest that the truncated genomes packaged into AAV2.7m8 trigger a more severe immune response. However, in the present study, we only evaluated outcomes six weeks post-IVT injection. Evaluation of retinas a few days following vector administration can potentially reveal whether innate immune responses are being triggered by AAV2.7m8 vectors. Profiling of immune cell populations in the retina at longer periods post-administration may also provide more information about vector-related responses. Nevertheless, further investigation to uncover the mechanisms by which truncated viral genome led to immunogenicity and inflammation will substantiate our findings and conclusions.

Finally, our observations suggest that not all 7-mer peptide insertions necessarily lead to a higher frequency of truncated genomes, as MyoAAV did not appear to exhibit multiple vector genome bands by alkaline gels (Fig. 2b). In this study, we did not further investigate the mechanism by which 7-mer inserts can cause genome packaging issues when AAV2 is used as the scaffold. AAV2 has been shown to be less thermostable than other serotypes [56–58]. Such peptide insertions and other alterations may exacerbate the stability of the AAV2 capsid, favoring particles with smaller genomes. The fact that that not all peptide inserts (including 7-mer sequences) at the 587–588 position are amenable to capsid assembly, is well documented [59, 60]. Alternatively, the peptide inserts may alter how the capsid protein interacts with Rep, resulting in the packaging of truncated genomes. Follow-up research is required to fully elucidate these processes.

Our findings raise somewhat of a paradox. AAV2.7m8 packages a higher degree of truncated and presumably inert genomes, yet it shows superior transduction of retinal tissues. The capsid itself was identified through selective enrichment following two rounds of in vivo screening for transducing photoreceptor cells [18]. The insertion also disrupts the basic arginine residues that are implicated in AAV2's binding to HSPGs. It has been hypothesized that disruption of the HSGP binding site permits better penetration/diffusion of the AAV2 scaffold capsid to the outer nuclear layers of the retina [61]. Alternatively, it has been observed that capsids with lower stabilities correlate with improved transduction, owning to more efficient uncoating and release of vector genomes [62, 63]. The genome heterogeneity observed for the AAV2.7m8 capsid may in fact be masking its full potential. Further improvements to limit vector heterogeneity are indeed warranted to enhance the safety and efficacies of eye gene therapy platforms using the AAV2.7m8 capsid.

DATA AVAILABILITY

The datasets generated and/or analyzed in the current study are available at the NCBI Sequence Read Archive (SRA) under the BioProject accession: PRJNA1127696.

REFERENCES

1. Bucher K, Rodriguez-Bocanegra E, Dauletbekov D, Fischer MD. Immune responses to retinal gene therapy using adeno-associated viral vectors - Implications for treatment success and safety. Prog Retin Eye Res. 2021;83:100915.
2. Kuzmin DA, Shutova MV, Johnston NR, Smith OP, Fedorin VV, Kukushkin YS, et al. The clinical landscape for AAV gene therapies. Nat Rev Drug Discov. 2021;20:173–4.
3. Wang D, Tai PWL, Gao G. Adeno-associated virus vector as a platform for gene therapy delivery. Nat Rev Drug Discov. 2019;18:358–78.
4. Sarkar H, Moosajee M. Choroideremia: molecular mechanisms and therapies. Trends Mol Med. 2022;28:378–87.
5. Ail D, Malki H, Zin EA, Dalkara D. Adeno-associated virus (AAV) - based gene therapies for retinal diseases: where are we? Appl Clin Genet. 2023;16:111–30.
6. Cideciyan AV, Jacobson SG, Beltran WA, Sumaroka A, Swider M, Iwabe S, et al. Human retinal gene therapy for Leber congenital amaurosis shows advancing retinal degeneration despite enduring visual improvement. Proc Natl Acad Sci USA. 2013;110:E517–25.
7. Russell S, Bennett J, Wellman JA, Chung DC, Yu ZF, Tillman A, et al. Efficacy and safety of voretigene neparvovec (AAV2-hRPE65v2) in patients with RPE65-mediated inherited retinal dystrophy: a randomised, controlled, open-label, phase 3 trial. Lancet. 2017;390:849–60.
8. Smalley E. First AAV gene therapy poised for landmark approval. Nat Biotechnol. 2017;35:998–9.
9. Xiong W, Wu DM, Xue Y, Wang SK, Chung MJ, Ji X, et al. AAV cis-regulatory sequences are correlated with ocular toxicity. Proc Natl Acad Sci USA. 2019;116:5785–94.
10. Chandler LC, McClements ME, Yusuf IH, Martinez-Fernandez de la Camara C, MacLaren RE, Xue K. Characterizing the cellular immune response to subretinal AAV gene therapy in the murine retina. Mol Ther Methods Clin Dev. 2021;22:52–65.
11. Jin E, Yin H, Li X, Zhao M. Short-term outcomes after intravitreal injections of conbercept versus ranibizumab for the treatment of retinopathy of prematurity. Retina. 2018;38:1595–604.
12. Sun Z, Zhou H, Lin B, Jiao X, Luo Y, Zhang F, et al. Efficacy and safety of intravitreal conbercept injections in macular edema secondary to retinal vein occlusion. Retina. 2017;37:1723–30.
13. Cheng SY, Luo Y, Malachi A, Ko J, Su Q, Xie J, et al. Low-dose recombinant adeno-associated virus-mediated inhibition of vascular endothelial growth factor can treat neovascular pathologies without inducing retinal vasculitis. Hum Gene Ther. 2021;32:649–66.
14. Liu K, Song Y, Xu G, Ye J, Wu Z, Liu X, et al. Conbercept for treatment of neovascular age-related macular degeneration: results of the randomized phase 3 PHOENIX study. Am J Ophthalmol. 2019;197:156–67.
15. Timmers AM, Newmark JA, Turunen HT, Farivar T, Liu J, Song C, et al. Ocular inflammatory response to intravitreal injection of adeno-associated virus vector: relative contribution of genome and capsid. Hum Gene Ther. 2020;31:80–9.
16. Ramlogan-Steel CA, Murali A, Andrzejewski S, Dhungel B, Steel JC, Layton CJ. Gene therapy and the adeno-associated virus in the treatment of genetic and acquired ophthalmic diseases in humans: Trials, future directions and safety considerations. Clin Exp Ophthalmol. 2019;47:521–36.
17. Drag S, Dotiwala F, Upadhyay AK. Gene therapy for retinal degenerative diseases: progress, challenges, and future directions. Invest Ophthalmol Vis Sci. 2023;64:39.
18. Dalkara D, Byrne LC, Klimczak RR, Visel M, Yin L, Merigan WH, et al. In vivo-directed evolution of a new adeno-associated virus for therapeutic outer retinal gene delivery from the vitreous. Sci Transl Med. 2013;5:189ra76.
19. Kern A, Schmidt K, Leder C, Muller OJ, Wobus CE, Bettinger K, et al. Identification of a heparin-binding motif on adeno-associated virus type 2 capsids. J Virol. 2003;77:11072–81.
20. Isgrig K, McDougald DS, Zhu J, Wang HJ, Bennett J, Chien WW. AAV2.7m8 is a powerful viral vector for inner ear gene therapy. Nat Commun. 2019;10:427.
21. Westhaus A, Cabanes-Creus M, Rybicki A, Baltazar G, Navarro RG, Zhu E, et al. High-throughput in vitro, ex vivo, and in vivo screen of adeno-associated virus

vectors based on physical and functional transduction. Hum Gene Ther. 2020;31:575–89.
22. Ramachandran PS, Lee V, Wei Z, Song JY, Casal G, Cronin T, et al. Evaluation of dose and safety of AAV7m8 and AAV8BP2 in the non-human primate retina. Hum Gene Ther. 2017;28:154–67.
23. Grishanin R, Vuillemenot B, Sharma P, Keravala A, Greengard J, Gelfman C, et al. Preclinical evaluation of ADVM-022, a novel gene therapy approach to treating wet age-related macular degeneration. Mol Ther. 2019;27:118–29.
24. Kiss S, Grishanin R, Nguyen A, Rosario R, Greengard JS, Nieves J, et al. Analysis of aflibercept expression in NHPs following intravitreal administration of ADVM-022, a potential gene therapy for nAMD. Mol Ther Methods Clin Dev. 2020;18:345–53.
25. Khanani AM, Thomas MJ, Aziz AA, Weng CY, Danzig CJ, Yiu G, et al. Review of gene therapies for age-related macular degeneration. Eye. 2022;36:303–11.
26. Heier JS, Kherani S, Desai S, Dugel P, Kaushal S, Cheng SH, et al. Intravitreous injection of AAV2-sFLT01 in patients with advanced neovascular age-related macular degeneration: a phase 1, open-label trial. Lancet. 2017;390:50–61.
27. Ye GJ, Budzynski E, Sonnentag P, Miller PE, Sharma AK, Ver Hoeve JN, et al. Safety and biodistribution evaluation in cynomolgus macaques of rAAV2tYF-CB-hRS1, a recombinant adeno-associated virus vector expressing retinoschisin. Hum Gene Ther Clin Dev. 2015;26:165–76.
28. Reichel FF, Dauletbekov DL, Klein R, Peters T, Ochakovski GA, Seitz IP, et al. AAV8 can induce innate and adaptive immune response in the primate eye. Mol Ther. 2017;25:2648–60.
29. Tai PWL, Xie J, Fong K, Seetin M, Heiner C, Su Q, et al. Adeno-associated virus genome population sequencing achieves full vector genome resolution and reveals human-vector chimeras. Mol Ther Methods Clin Dev. 2018;9:130–41.
30. Su Q, Sena-Esteves M, Gao G. Purification of recombinant adeno-associated viruses (rAAVs) by cesium chloride gradient sedimentation. Cold Spring Harb Protoc. 2020;2020:095604.
31. Grieger JC, Soltys SM, Samulski RJ. Production of recombinant adeno-associated virus vectors using suspension HEK293 cells and continuous harvest of vector from the culture media for GMP FIX and FLT1 clinical vector. Mol Ther. 2016;24:287–97.
32. Sanmiguel J, Gao G, Vandenberghe LH. Quantitative and digital droplet-based AAV genome titration. Methods Mol Biol. 2019;1950:51–83.
33. Su Q, Sena-Esteves M, Gao G. Analysis of recombinant adeno-associated virus (rAAV) purity using silver-stained SDS-PAGE. Cold Spring Harb Protoc. 2020;2020:095679.
34. Tran NT, Lecomte E, Saleun S, Namkung S, Robin C, Weber K, et al. Human and insect cell-produced recombinant adeno-associated viruses show differences in genome heterogeneity. Hum Gene Ther. 2022;33:371–88.
35. Afgan E, Sloggett C, Goonasekera N, Makunin I, Benson D, Crowe M, et al. Genomics virtual laboratory: a practical bioinformatics workbench for the cloud. PLoS ONE. 2015;10:e0140829.
36. Blankenberg D, Von Kuster G, Coraor N, Ananda G, Lazarus R, et al. Galaxy: a web-based genome analysis tool for experimentalists. Curr Protoc Mol Biol. 2010; Chapter 19:Unit 19.10.1-21.
37. Giardine B, Riemer C, Hardison RC, Burhans R, Elnitski L, Shah P, et al. Galaxy: a platform for interactive large-scale genome analysis. Genome Res. 2005;15: 1451–5.
38. Goecks J, Nekrutenko A, Taylor J, Galaxy T. Galaxy: a comprehensive approach for supporting accessible, reproducible, and transparent computational research in the life sciences. Genome Biol. 2010;11:R86.
39. Robinson JT, Thorvaldsdottir H, Winckler W, Guttman M, Lander ES, Getz G, et al. Integrative genomics viewer. Nat Biotechnol. 2011;29:24–6.
40. Deverman BE, Pravdo PL, Simpson BP, Kumar SR, Chan KY, Banerjee A, et al. Cre-dependent selection yields AAV variants for widespread gene transfer to the adult brain. Nat Biotechnol. 2016;34:204–9.
41. Tabebordbar M, Lagerborg KA, Stanton A, King EM, Ye S, Tellez L, et al. Directed evolution of a family of AAV capsid variants enabling potent muscle-directed gene delivery across species. Cell. 2021;184:4919–38 e22.
42. Chan KY, Jang MJ, Yoo BB, Greenbaum A, Ravi N, Wu WL, et al. Engineered AAVs for efficient noninvasive gene delivery to the central and peripheral nervous systems. Nat Neurosci. 2017;20:1172–9.
43. Xie J, Mao Q, Tai PWL, He R, Ai J, Su Q, et al. Short DNA hairpins compromise recombinant adeno-associated virus genome homogeneity. Mol Ther. 2017;25:1363–74.
44. Hirata RK, Russell DW. Design and packaging of adeno-associated virus gene targeting vectors. J Virol. 2000;74:4612–20.
45. Chan YK, Wang SK, Chu CJ, Copland DA, Letizia AJ, Costa Verdera H, et al. Engineering adeno-associated viral vectors to evade innate immune and inflammatory responses. Sci Transl Med. 2021;13:eabd3438.
46. Murenu E, Gerhardt MJ, Biel M, Michalakis S. More than meets the eye: the role of microglia in healthy and diseased retina. Front Immunol. 2022;13:1006897.
47. Tummala G, Crain A, Rowlan J, Pepple KL. Characterization of gene therapy associated uveitis following intravitreal adeno-associated virus injection in mice. Invest Ophthalmol Vis Sci. 2021;62:41.
48. Sahel JA, Boulanger-Scemama E, Pagot C, Arleo A, Galluppi F, Martel JN, et al. Partial recovery of visual function in a blind patient after optogenetic therapy. Nat Med. 2021;27:1223–9.
49. Li C, Goudy K, Hirsch M, Asokan A, Fan Y, Alexander J, et al. Cellular immune response to cryptic epitopes during therapeutic gene transfer. Proc Natl Acad Sci USA. 2009;106:10770–4.
50. Keiser MS, Ranum PT, Yrigollen CM, Carrell EM, Smith GR, Muehlmatt AL, et al. Toxicity after AAV delivery of RNAi expression constructs into nonhuman primate brain. Nat Med. 2021;27:1982–9.
51. Brimble MA, Cheng PH, Winston SM, Reeves IL, Souquette A, Spence Y, et al. Preventing packaging of translatable P5-associated DNA contaminants in recombinant AAV vector preps. Mol Ther Methods Clin Dev. 2022;24:280–91.
52. Olson JK, Miller SD. Microglia initiate central nervous system innate and adaptive immune responses through multiple TLRs. J Immunol. 2004;173:3916–24.
53. Wright JF. Quantification of CpG motifs in rAAV genomes: avoiding the toll. Mol Ther. 2020;28:1756–8.
54. Grootjans J, Kaser A, Kaufman RJ, Blumberg RS. The unfolded protein response in immunity and inflammation. Nat Rev Immunol. 2016;16:469–84.
55. Muhuri M, Maeda Y, Ma H, Ram S, Fitzgerald KA, Tai PW, et al. Overcoming innate immune barriers that impede AAV gene therapy vectors. J Clin Invest. 2021;131:e143780.
56. Horowitz ED, Rahman KS, Bower BD, Dismuke DJ, Falvo MR, Griffith JD, et al. Biophysical and ultrastructural characterization of adeno-associated virus capsid uncoating and genome release. J Virol. 2013;87:2994–3002.
57. Pacouret S, Bouzelha M, Shelke R, Andres-Mateos E, Xiao R, Maurer A, et al. AAV-ID: a rapid and robust assay for batch-to-batch consistency evaluation of AAV preparations. Mol Ther. 2017;25:1375–86.
58. Hsu HL, Brown A, Loveland AB, Lotun A, Xu M, Luo L, et al. Structural characterization of a novel human adeno-associated virus capsid with neurotropic properties. Nat Commun. 2020;11:3279.
59. Zhu D, Brookes DH, Busia A, Carneiro A, Fannjiang C, Popova G, et al. Optimal trade-off control in machine learning-based library design, with application to adeno-associated virus (AAV) for gene therapy. Sci Adv. 2024;10:eadj3786.
60. Douar AM, Poulard K, Danos O. Deleterious effect of peptide insertions in a permissive site of the AAV2 capsid. Virology. 2003;309:203–8.
61. Khabou H, Desrosiers M, Winckler C, Fouquet S, Auregan G, Bemelmans AP, et al. Insight into the mechanisms of enhanced retinal transduction by the engineered AAV2 capsid variant -7m8. Biotechnol Bioeng. 2016;113:2712–24.
62. Pavlou M, Schon C, Occelli LM, Rossi A, Meumann N, Boyd RF, et al. Novel AAV capsids for intravitreal gene therapy of photoreceptor disorders. EMBO Mol Med. 2021;13:e13392.
63. Rode L, Bar C, Gross S, Rossi A, Meumann N, Viereck J, et al. AAV capsid engineering identified two novel variants with improved in vivo tropism for cardiomyocytes. Mol Ther. 2022;30:3601–18.

ACKNOWLEDGEMENTS

We would like to extend our thanks to Shun-Yun Cheng for her generous guidance, technical training, and support. We would also like to thank the UMass Chan Deep Sequencing core (Maria Zapp, Daniella Wilmot, and Ellie Kittler) for their help with sample preparations and SMRT sequencing.

AUTHOR CONTRIBUTIONS

MC, GG, and PWLT conceived and designed the study; MC, QS, MY, and JM acquired the data; MC, QS, MY, GG, CP, and PWLT analyzed and interpreted the results; MC, CP, and PWLT drafted and revised the manuscript; GG and PWLT approved and finalized the manuscript. All authors have agreed to be accountable for all aspects of the work in ensuring that questions related to the accuracy or integrity of any part of the work are appropriately investigated and resolved.

FUNDING

GG is supported by grants from the UMass Chan Medical School (an internal grant) and by the National Institutes of Health (R01NS076991-01, P01HL131471-05, R01AI121135, UG3HL147367-01, R01HL097088, R01HL152723-02, U19AI149646-01, and UH3HL147367-04). PWLT is supported by an award from The Bassick Family Foundation, and a BRIDGE Fund Award (a UMass Chan Medical School internal grant).

COMPETING INTERESTS

GG is a scientific co-founder of Voyager Therapeutics and Aspa Therapeutics and holds equity in these companies. GG and PWLT are inventors on patents with royalties licensed to biopharmaceutical companies. GG, CP, and PWLT also received sponsored research support from Kanghong Pharmaceuticals for unrelated research. The remaining authors declare no competing interests.

ETHICAL APPROVAL

All mouse experiments were conducted at UMass Chan Medical School following protocols and procedures and were approved by the UMass Chan Medical School Institutional Animal Care and Use Committee.

ADDITIONAL INFORMATION

Supplementary information The online version contains supplementary material available at https://doi.org/10.1038/s41434-024-00477-7.

Correspondence and requests for materials should be addressed to Guangping Gao or Phillip W. L. Tai.

Reprints and permission information is available at http://www.nature.com/reprints

Publisher's note Springer Nature remains neutral with regard to jurisdictional claims in published maps and institutional affiliations.

Table S1. Summary of vector titers

Vector ID	Vector construct	Source of *trans* plasmid	Source of *cis* plasmid	Titer (vg/mL)
VCAV-8051	scAAV2-*CB6-Egfp*	Aldevron	Synbio Technologies	4.12E+12
VCAV-8050	scAAV2.7m8-*CB6-Egfp*	In-house CsCl preparation	Synbio Technologies	5.09E+12
VCAV-4305	ssAAV2-*CB6-Egfp*	Aldevron	Synbio Technologies	4.00E+12
VCAV-7763	ssAAV2.7m8-*CB6-Egfp*	In-house CsCl preparation	Synbio Technologies	5.15E+12
VCAV-8310	ssAAV2-*CB6-FLuc*	Aldevron	In-house CsCl preparation	3.09E+12
VCAV-8546	ssAAV2.7m8-*CB6-FLuc*	In-house CsCl preparation	In-house CsCl preparation	7.50E+12
VCAV–09315	scAAV2.7m8A.CB6-Egfp	In-house CsCl preparation	Synbio Technologies	1.04E+12
VCAV–09316	scAAV2.7m8B.CB6-Egfp	In-house CsCl preparation	Synbio Technologies	2.19E+12
VCAV–09317	scAAV2.7m8C.CB6-Egfp	In-house CsCl preparation	Synbio Technologies	1.38E+12
ALR-159	AAV9-2xsup-tRNA-*CB6-mCherry*	Aldevron	In-house CsCl preparation	9.00E+12
ALR-163/164	MyoAAV-2xsup-tRNA-*CB6-mCherry*	In-house CsCl preparation	In-house CsCl preparation	8.22E+12
VCAV-6361	ssAAV9.*Egfp*	Aldevron	In-house CsCl preparation	3.13E13
VCAV-6864	ssAAV9.PHPeB.*Egfp*	In-house CsCl preparation	In-house CsCl preparation	2.00E13

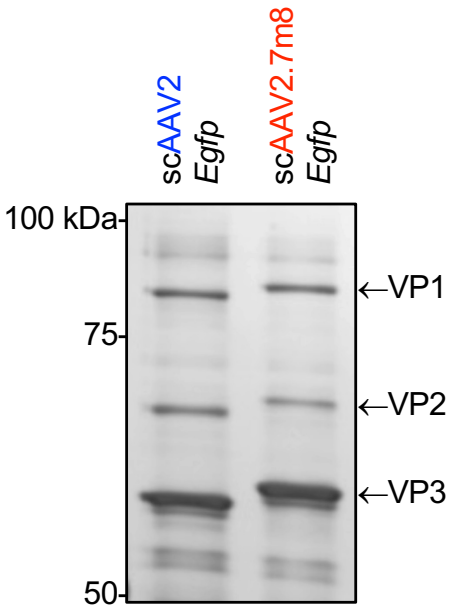

Fig. S1. Silver-stained poly-acrylamide gel of the scAAV-*Egfp and* ssAAV-*Egfp* vectors. The predominant capsid bands (VP1, VP2, and VP3) are indicated.

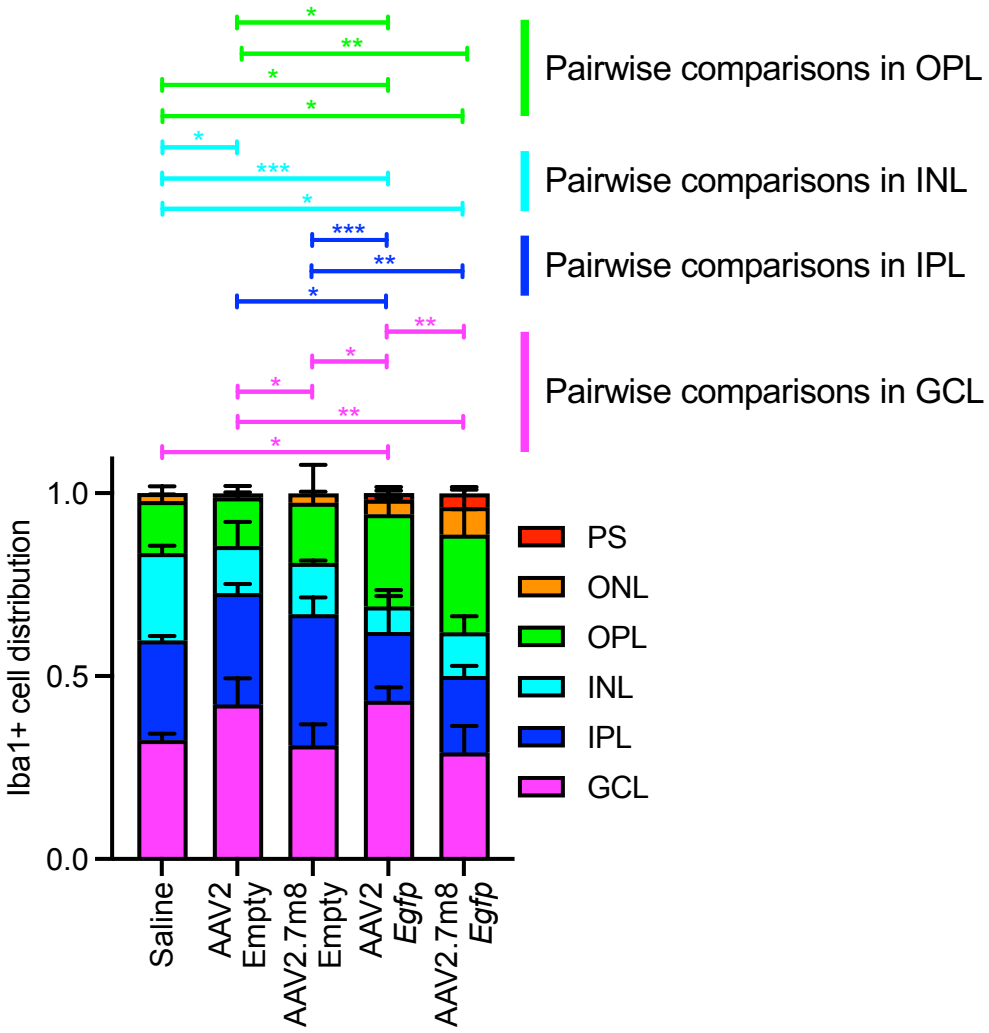

Fig. S2. Distributions of microglia in AAV-treated retinas. Counts of microglia (IBA1+) in each retinal layer from **Fig. 3d** were expressed as a fraction of all IBA+ cells in retinal cross-sections and plotted as a stacked histogram. Photoreceptor segment layer, (PS); outer nuclear layer (ONL); outer plexiform layer (OPL); inner nuclear layer (INL); inner plexiform layer (IPL); ganglion cell layer (GCL). n=3. Values = means ±SD. *p<0.05, **p<0.01, ***p<0.001, 2way ANOVA with Tukey's method for multiple comparisons